MEASUREMENTS OF THE ACCELERATION OF REFLECTED SHOCK WAVES BY MEANS OF A NEW HEAT TRANSFER GAUGE

Thesis by

Erik Slachmuylders

In Partial Fulfillment of the Requirements

For the Degree of

Aeronautical Engineer

California Institute of Technology

Pasadena, California

1963

ACKNOWLEDGMENT

The author gratefully realizes that the active interest and the enthusiasm of Professor Hans W. Liepmann during the course of this work have been extremely helpful to complete the work described in this paper.

Much cooperation was received from Professors Bradford Sturtevant and Anatol Roshko; the former initiated the author in the operation of the 17-inch shock tube. This is acknowledged with sincere gratitude.

Mrs. Geraldine Krentler transformed the manuscript into its final form under rather inconvenient conditions.

This research was supported by the National Aeronautics and Space Administration under Grant Number NsG-40-60.

ABSTRACT

A small heat transfer probe, operating in the free molecule flow regime, was developed with the purpose of obtaining accurate x, t diagrams of a reflected shock wave close to the end wall of the GALCIT 17-inch shock tube.

The sensitive element of the probe consists of a .005" diameter filament of non-conducting material coated with a thin metallic film. The sensitivities of a filament probe and a conventional cold wire are compared analytically and it is found that the filament probe has favorable characteristics for measurement times of the order of a few microseconds. This is confirmed by the experiments.

The probe was mounted in the end wall of the 17-inch shock tube and x, t diagrams of reflected shock waves were measured at three levels of the initial pressure. The initial motion of the reflected shock is governed by heat loss to the reflecting wall; the wave velocity approaches its ideal value only asymptotically. The asymptotic approach agrees closely with the results of a boundary layer theory. The measurements indicate that the trajectory of the reflected shock wave close to the end wall is characterized by three different regions; the region in which boundary layer theory is valid, a region closer to the wall in which deviations from boundary layer theory are observed, and a non-continuum region adjacent to the wall in which the reflected shock is formed. The reflected shock wave is found to leave the formation region with a velocity which is approximately 20 per cent

below the ideal velocity. It then accelerates toward this ideal velocity, approaching within 3 per cent at distances from the end wall of about 1000 mean free paths. The boundary layer approximation is found to be valid for distances greater than about 70 mean free paths. Accordingly, a non-uniform temperature profile is to be expected in a layer of approximately 100 mean free paths from the end wall.

TABLE OF CONTENTS

LIST OF TABLES AND FIGURES

LIST OF SYMBOLS

a	Radius
c	Specific heat
D	Diameter expressed in mils
k	Coefficient of thermal conductivity
$\varkappa$	Coefficient of thermal diffusivity. $\varkappa = k/\rho c$
L	Length of sensitive element of probe
M_s	Mach number of incident shock wave
p	Pressure
q	Heat flux per unit area and time
r	Electrical resistance per unit length of probe
$s = U/v_m$	Molecular speed ratio
t_i	Instant of passage of incident shock over probe
t_r	Instant of passage of reflected shock over probe
t_o	Instant of impact of incident wave on end wall
$t^* = \frac{t_r - t_o}{\Lambda_2 / u_{R,I}}$	Non-dimensional time
T_s	Surface temperature of filament
$u_{R,I}$	Ideal reflected shock speed
u_R	Actual reflected shock speed
u_s	Velocity of incident shock wave
v_m	Most probable molecular speed
w	Joule heat dissipated per unit length of probe
$x^* = x/\Lambda_2$	Non-dimensional distance from end wall

LIST OF SYMBOLS (CONTD.)

α	Temperature coefficient of resistivity or Accommodation coefficient
δ	Thickness of thermal layer
ΔE	Signal output of probe
θ	Orientation angle of the film with respect to the flow direction
λ	Shock thickness
Λ	Mean free path
ρ	Density
σ	Coefficient of electrical resistivity
τ	Time expressed in microseconds

Subscripts

o	Refers to the initial conditions of the filament, just before the passage of the incident shock
1	Refers to the initial conditions of the test gas
2	Refers to the conditions in the region behind the incident shock
5	Refers to the conditions behind the reflected shock
b	Refers to properties of the filament material
f	Refers to properties of the film itself
w	Refers to properties of the wire or end wall

I. INTRODUCTION

This paper reports the development and application of a small heat transfer probe for studying rarefied gas flows. The probe, a cylindrical non-conducting filament coated with a thin metallic film, is an outgrowth of the conventional hot wire (more precisely called a "cold wire" in shock tube applications). It has sufficient sensitivity and time response to be applicable to the measurements of the profile of moving shock waves in shock tubes. In the current investigation the thin-film-coated filament has been used as a timing device to study the propagation of shock waves very close to the end wall of the shock tube.

It is clear that in both of these applications the very short time it takes a shock to pass over a fixed point (the shock passage time) creates severe instrumentation problems. In shock tubes which operate in the mm range of pressure these problems have so far been insurmountable, but with the construction of the GALCIT 17-inch shock tube (Ref. 1), especially designed for operation at very low pressures, shock thicknesses of up to 5 mm and passage times of from 1 to 5 μ sec can be obtained. It is clear that this is a major improvement.

The use of the cold wire in shock tube flows has been investigated by W. H. Christiansen (Ref. 2) and the limitations and possibilities of this probe were thoroughly considered by him. The cold wire is distinguished by the fact that the interpretation of its signal presents no important problems. Furthermore, it is comparatively easily made and does not require prohibitively cumbersome calibration procedures.

The sensitivity of the cold wire probe, however, is completely determined by its diameter and the material from which it is made. For measurements in the flow region behind a shock wave the sensitivity of the cold wire probe is satisfactory, but, as was pointed out in reference 2, measurements of the profile of thick moving shock waves by means of a cold wire may be hampered by lack of sensitivity and time response. Both the small amplitude * of the signal produced by the cold wire and the very short characteristic time of the phenomenon may necessitate restrictively high electronic amplification.

For that reason an attempt has been made to develop a probe similar to a cold wire but with increased sensitivity. The cold wire has been replaced by a filament of about 5 mil diameter coated with a very thin metallic film (100 - 500 $\mathring{A}$). It will be shown that this element possesses a higher sensitivity than the conventional wire for times comparable to the shock passage time. This feature makes the coated filament a very promising instrument not only for analysis of the structure of a moving shock wave but also for experiments requiring accurate timing of the shock passage.

The purpose of the following section is to analyze the behavior of a coated filament, to establish its sensitivity and to compare this with the sensitivity obtained by a conventional cold wire. Furthermore, a method is discussed which would allow separation of the variables (ρ, T, M) in the moving shock by means of 3 simultaneous measurements. It is interesting to note that those 3 measurements can be carried out by one single filament coated with 3 independent films.

---

* It is shown in reference 2 that the output of a cold wire probe in a moving shock is essentially independent of the initial pressure.

II. CHARACTERISTICS OF THIN-FILM COATED FILAMENTS

Before dealing with the characteristics of film-coated filaments it might be useful to point out the fundamental difference between the cold wire and the film-coated filament. The cold wire is operated in such a manner that the temperature change can be considered uniform over the cross section (Ref. 2). Therefore, the signal output of the cold wire is proportional to the average temperature change throughout the complete wire.

On the other hand, with a film-coated filament the resistance element is formed by the thin film of conducting material which is deposited (usually by means of evaporation) onto a non-conducting filament (usually quartz or Pyrex). Therefore, the signal output of the filament probe will be proportional to the temperature change of this thin surface layer. It will be important for the purposes of analysis to operate the filament probe in such a way that only a small shell near the surface is affected by the heat transferred from the fluid to the filament.

The fact that the output of the film gauge is related to the surface temperature of the filament whereas the output of the cold wire is determined by the temperature change of the whole body, explains the major difference in response between the two gauges. In this section the temperature response of a film-coated filament will be studied and a comparison will be made with the conventional cold wire.

A. Temperature Response of a Film-Coated Filament.

The thin film resistance thermometer is a well known and widely used instrument for transient heat transfer measurements. An excellent description of this technique with references to the vast literature on this subject can be found in references 3 and 4. For most conditions encountered in the shock tube one can consider the body onto which the film is deposited, as a semi-infinite slab. It will be shown here that the same assumption remains valid for a thin filament over time intervals of the order of the shock passage time.

Consider the cross section of a cylindrical filament of radius a, coated with a conducting film of thickness Δ. Neglecting the (small) heat flux in the axial direction and assuming uniform conditions in the θ-direction, the equation for the heat conduction inside the body is:

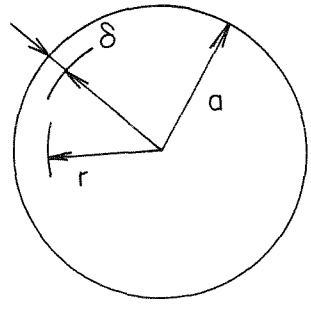

$$r \frac{\partial T}{\partial t} = \varkappa \frac{\partial}{\partial r} \left(r \frac{\partial T}{\partial r} \right), \quad \left(\varkappa = \frac{k}{\rho c} \right) \tag{1}$$

with

$$k \left. \frac{\partial T}{\partial r} \right|_{r=a} = q \tag{2}$$

The equations being linear, it is sufficient to know the response to a step function of the heat influx q per unit area and time. The exact solution (Ref. 5) can be expressed as the sum of an infinite

series of Bessel functions. Since the form of the solution does not give a physical insight into the problem, an approximate solution will be given using integral methods well known in the study of boundary layers. This will clearly show the applicability of the results of the heat conduction in a one-dimensional semi-infinite slab, and at the same time it will yield a criterion for the limit of the validity of those results.

Making the assumption that all heat which is gained by the filament affects only a thin shell near the surface one can introduce a penetration parameter $\delta(t)$. In addition the following temperature profile is assumed

$$T(r, t) = T_0 + [\, T_s(t) - T_0 \,] \left[1 - \frac{a - r}{\delta} \right]^2 \tag{3}$$

where T_s is the surface temperature of the filament and T_0 is the initial uniform temperature of the filament. Integrating equation 1 over the penetrated shell one obtains

$$\int_{a-\delta(t)}^{a} r \frac{\partial T}{\partial t}\, dr = \kappa \int_{a-\delta(t)}^{a} \frac{\partial}{\partial r} \left(r \frac{\partial T}{\partial r} \right) dr \tag{4}$$

Introducing equation 3 into equation 4 one obtains

$$\frac{d}{dt} \left[T_0 \left(a\delta - \frac{\delta^2}{2} \right) + (T_s - T_0) \left(\frac{a\delta}{3} - \frac{\delta^2}{12} \right) \right] - (a - \delta) T_0 \frac{d\delta}{dt} = \kappa\, a \left. \frac{\partial T}{\partial r} \right|_{r=a} \tag{5}$$

This equation still contains the 2 unknowns $\delta(t)$, $T_s(t)$ which are related through the boundary conditions

$$q = k\frac{\partial T}{\partial r}\Big)_{r=a} = \frac{2k(T_s - T_0)}{\delta} \tag{6}$$

Elimination of $(T_s - T_0)$ between equations 5 and 6 yields a differential equation for $\delta(t)$, which can be integrated to give

$$\frac{2\kappa t}{a^2} = \frac{\delta}{a}\left(\frac{\delta}{3a} - \frac{\delta^2}{12a^2}\right) \tag{7}$$

Consider the case where $\delta/a \leq 0.1$. Then $\frac{\delta}{3a} \gg \frac{\delta^2}{12a^2}$ and equation 7 becomes

$$\delta \doteq \sqrt{6\kappa t}$$

From equations 6 and 7 the surface temperature is given by

$$T_s - T_0 = \frac{q\delta}{2k} = \frac{q\sqrt{6\kappa t}}{2k} = 1.22\,\frac{q\sqrt{t}}{\sqrt{k\rho c}} \tag{8}$$

This can be compared with the solution for the one-dimensional heat conduction in a semi-infinite slab, where

$$T_s - T_0 = \frac{2}{\sqrt{\pi}}\,\frac{q\sqrt{t}}{\sqrt{k\rho c}} = 1.13\,\frac{q\sqrt{t}}{\sqrt{k\rho c}} \tag{9}$$

As could be expected, the effects of the finite size and curvature of the filament are completely negligible initially, and the surface of the filament heats up initially as if it were backed by an infinite body. The limit of the validity of the one-dimensional results can be determined from the condition $\delta / a \ll 0.1$ which yields

$$t_{max} = \frac{a^2}{600\,\kappa} \tag{10}$$

For quarts $\kappa \doteq 6 \times 10^{-3} \ \frac{cm^2}{sec}$ and t_{max} becomes

$$\tau_{max} = 0.4\, D^2, \quad \tau_{max} \text{ in } \mu\text{sec.} \tag{10a}$$

D = diameter of the filament in mils.

For a 5 mil filament this gives $\tau_{max} = 10\ \mu$ sec.

A comparison has been made between the exact solution, the one-dimensional solution, and the approximate integral solution. For a 4 mil diameter quartz filament and $\tau = 5\ \mu$ sec. ($\tau = 0.8\ \tau_{max}$) one obtains

$$\frac{T_s - T_0}{q} = \begin{cases} 69.4 \times 10^{-3} & \text{(exact solution)} \\ 70.0 \times 10^{-3} & \text{(one-dim. solution)} \\ 75.5 \times 10^{-3} & \text{(approx. solution)} \end{cases}$$

Even at 80 per cent of the maximum time the agreement between the one-dimensional solution and the exact solution is very good and even better agreement can be expected for either shorter times or thicker filaments.

It is useful to compare t_{max} with the shock passage time t_s

$$t_s = \frac{\lambda}{M_s a_1} = \frac{\frac{\lambda}{d} \cdot d}{M_s a_1}$$

where λ is the shock thickness and d is the tube diameter. Assuming Argon as test gas in the 17-inch shock tube $\tau_s = 1.36 \times 10^3 \frac{\lambda/d}{M_s}$. The following table gives λ/d and τ_s vs. M_s for $p_1 = 30$ μ Hg in Argon (λ/d is taken from Ref. 1). It is clear that for these conditions a 5 mil diameter filament will behave as a semi-infinite slab during the time of the passage of the shock wave.

TABLE I

Shock Passage Time in Argon for $p_1 = 30$ μHg.

M_s	$\lambda/d \times 10^2$	τ_s (μsec.)
2	1.55	10.5
4	1.12	3.81
6	1.22	2.76
8	1.33	2.26
10	1.45	1.97

B. Comparison of the Sensitivity of a Thin Metallic Wire (cold wire) and a Thin-Film Coated Filament.

In this section a comparison is made of the responses of a thin metallic wire and of a coated filament to a step increase in the heat flux q. It will be shown that for measurement times of the order of the shock passage time the filament has a better response than the wire. Therefore, it seems to be the appropriate instrument with which to analyse the shock structure or accurately time the motion of a moving shock wave. (A few of the latter type of measurement were made by Christiansen, (Ref. 2).)

In view of the intended experiments (analysis of the structure of a moving shock and accurate timing of the reflected shock from the end wall), the diameter of either the wire or the filament must not exceed a fraction of the mean free path in the gas ahead of the shock. If this condition is satisfied the probes will operate in the free-molecule flow regime (Refs. 6 and 7). In free-molecule flow the heat influx q is uniquely determined by the state of the gas, local Mach number, surface temperature and orientation of the surface. Throughout this comparison it will be assumed that the heat influx per unit area is equal for both kinds of probe. Furthermore, since the sensitivity of the cold wire probe is proportional to the combination $\frac{\sigma\alpha}{\rho c}$ (Ref. 2) and since this factor does not vary much for the conventional wire materials, the comparison will be made between a Platinum wire (chosen as a representative wire) and a Platinum-coated quartz filament. The following comparison is carried out for the conditions occurring in the 17-inch shock tube.

The basic equation for the signal output of a resistance gauge is $\Delta E = RI\alpha\,\Delta T$ (it is assumed that the gauge is operated at constant current). In order to compare wire with filament it is useful to write ΔE in a different way,

$$\Delta E = \sqrt{r\,w}\quad L\ \alpha\ \Delta T$$

(r, w represent the resistance and the Joule heat dissipated per unit length of the probe; L is the length of the sensitive element). Each one of the factors appearing in the expression for ΔE will now be treated separately in order to illustrate the points of difference. For the purposes of the comparison we will assume that the preheat of the element is not large (that is, that the initial element temperature is not much above room temperature). This greatly simplifies the analysis of gauge output but may turn out to be an unnecessary restriction in practice.

a) ΔT: Temperature change of the sensitive element.

It should be noted that in the case of a wire ΔT represents the average temperature change of the complete wire, whereas in the case of a filament ΔT represents the change of the surface temperature. Assuming no axial heat flow and uniform temperature over the cross section of the wire, the temperature of the wire is

$$\Delta T = \frac{4\,qt}{\rho_w\, c_w\, d_w}$$

In section II. A it is shown that for sufficiently short times

the filament behaves as a semi-infinite body, and the surface temperature is given by

$$\Delta T_s = \frac{2}{\sqrt{\pi}} \frac{q\sqrt{t}}{\sqrt{k_b \rho_b c_b}}$$

This gives for the gauges being compared

$$\frac{\Delta T_s}{\Delta T_w} = 15 \frac{D}{\sqrt{\tau}}$$

where D is the diameter of the wire expressed in mils and τ the time in μ sec. This ratio is time dependent due to the different time behavior of the film and wire temperature (Eq. 9). For a 0.1 mil wire the ratio becomes 1 for a time slightly larger than 1 μ sec.

b) r: Resistance per unit length.

For the wire this resistance is $r_w = \frac{4\sigma_w}{\pi d_w^2}$. For the filament, uniformly coated over its entire surface

$$r_f = \frac{\sigma_f}{\pi d_b \Delta}$$

where Δ is the film thickness. By experience it was found that a film thickness $\Delta = 100$ $\mathring{A}$ (based on the bulk coefficient of resistivity for the material used) is a lower limit below which the properties of the films are not reproducible (negative or zero temperature coefficient). In this case the ratio of the resistances per unit length

becomes

$$\frac{r_f}{r_w} = \frac{d_w^2}{4d_b\Delta}$$

(assuming the same value for σ_f and σ_w)

This ratio becomes equal to 1 for $D_w = 0.1$ and $D_f = 6$. It is clear that the resistance per unit length on the filament can be improved considerably by coating a small portion of the contour of the filament.

c) α : Temperature coefficient of resistivity.

It is found in practice that for both thin wires and thin films α is well below the bulk value of the material used. For a number of Pt-coated filaments α was measured over wide temperature ranges; it remained constant for each filament but appreciable variation was found in successive samples. The measured α varied from 0.0015 to 0.0025 whereas the bulk coefficient is 0.0039.

d) L: Length of the filament or wire.

The length of the sensitive element of the probes is determined by either mechanical strength or by conditions imposed by shock curvature, shock tube dimensions, etc. By experience it was found that the filaments could be made as long as 3/4" without suffering frequent breakage*. (It should be noted that the filaments break mainly due to vibration of the needles; the use of stiffer needles would be a definite improvement.) They were not made any longer because this

* In fact, with 3 filaments in the tube as many as 20 consecutive runs were made without breaking any filament.

could introduce timing errors due to the shock curvature. The same limitation holds for wires with enough mechanical strength. For thinner wires the length of the wire will have to be reduced accordingly*.

e) w: Joule heat dissipated per unit length.

We assume that for measurements with a cold resistance probe the temperature difference between the surrounding gas and the probe due to Joule heating is kept small. This temperature difference can be reduced by reducing the excitation current and thus the Joule heating. Since this affects the signal output of the probe, it is important to know the allowable Joule heating for a given temperature difference between gas and probe.

The Joule heat produced in the probe is carried away by 3 processes: convection to the gas, conduction to the supports and radiation. Assuming small temperature differences between the sensitive element and the surrounding gas as well as between the center of the sensitive element and its supports, the modes of heat transfer can be considered separately and then be added.

e. 1) Conduction to the supports.

For all applications one can assume the support temperature equal to the gas temperature T_1; the equation of steady heat conduction becomes then:

$$\frac{\pi d^2 k}{4} \frac{d^2(T - T_1)}{dx^2} = - I^2 r \left[1 + \alpha (T - T_1) \right]$$

* Recent experiments in the 17-inch shock tube with 0.01 mil Pt-Rh wires have shown that lengths of approximately 1/20" may be used, at tube pressures below 100 microns Hg.

In view of the small temperature differences one can drop the term $\alpha (T - T_1)$; this leads to a parabolic temperature profile along the sensitive element. The average temperature difference between this element and the gas is then

$$\overline{T - T_1} = \frac{w L^2}{3 d^2 k} \qquad \text{or} \qquad w = \frac{3 d^2 k}{L^2} \overline{(T - T_1)}$$

e. 2) Convection from probe to surrounding gas before a run.

As was pointed out before, the diameter of either probe is small compared to the mean free path in the surrounding gas, and the heat convected to the gas can be calculated from the free-molecule heat transfer equation (Ref. 6)

$$q = \frac{\alpha\sqrt{2}}{\sqrt{\pi \gamma}} \; p_1 a_1 T_1 \left[\overline{T - T_1}\right]$$

Here α is the so-called accommodation coefficient, assumed = 1. For a typical case of Argon at 50 μ Hg and room temperature this gives

$$q \doteq 10^{-4} \overline{(T - T_1)} \quad \frac{\text{cal}}{\text{cm}^2 \text{sec}}$$

or, expressing this in the form of an energy per unit length of

the probe,

$$w_{conv} = \pi d \, 10^{-4} \, (\overline{T - T_1}) \quad \frac{cal}{cm \, sec}$$

e.3) Heat losses due to radiation.

Since we have assumed that the cold resistance thermometer is operated with a small preheat, it is clear that the heat lost through radiation can be neglected in most cases.

The allowable Joule heating per unit length of the probe can then be written as

$$w = w_{cond} + w_{conv} = \left(\frac{3dk}{L^2} + A\right) \pi d \, \overline{(T - T_1)}$$

where A is a constant depending on the state of the gas surrounding the probe. w has been computed for a few typical cases and is given in the following table together with the other factors appearing in the equation

$$\Delta E = \alpha \sqrt{r w} \quad L \, \Delta T$$

TABLE II

Comparison of the Signal Output of a 5 mil Diameter Platinum-coated Quartz Filament and a Platinum Cold Wire (1, 0.1, 0.5 and 0.01 mil diameter) for t = 1 μ sec.

	$D_w = 1$	$D_w = 0.1$	$D_w = 0.05$	$D_w = 0.01$
L_f/L_w	1	1	2	10
$\sqrt{r_f/r_w}$	10	1	0.5	0.1
$\sqrt{w_f/w_w}$	1	7	9	15
$\Delta T_f/\Delta T_w$	10	1	0.5	0.1
$\Delta E_f/\Delta E_w$	100	7	4.5	1.5

The results are given as the ratio of the value of a factor computed for a quartz filament (D = 5 mil) coated with Platinum (film thickness: 100 $\mathring{A}$), to the value of the same factor computed for a wire. It should be noted that the ratio of the temperature changes is time dependent due to the parabolic temperature response of the filament. The ratio given in the table corresponds to t = 1 μ sec after the step in q is applied. The initial gas condition is: Argon at 50 μHg and 300°K. This table clearly shows that the high sensitivity of the film-coated filament stems from its long length and large heat dissipation. It should be noted that for times shorter than 1 μ sec the relative sensitivity of the film gauge becomes even better due to the parabolic behavior of the film gauge output.

It is concluded that for analysis of the structure of a moving

shock wave or accurate timing of this wave the film probe seems to be the appropriate instrument. An actual comparison of the responses of a wire and a filament is shown in Figure 1.a. The conditions are: $p_1 = 500$ μ Hg and $M_s = 4.16$. The upper trace shows the output of a .01 mil wire, 1/20" long, with a cold resistance of 4.4K and operated under a constant current of 90 μA. The output of the filament probe is displayed on the lower trace. The characteristic constants of the filament are: diameter 5 mil; length, 3/4"; material, Pyrex coated with Platinum; cold resistance, 400 ohm, and a constant current of 8 mA.

The picture shows a definite superiority of the filament probe over the cold wire, especially for the first few microseconds. At the same time it illustrates the fundamental difference in behavior between a wire and a filament. The output of the wire is essentially linear, whereas the output of the probe is nearly parabolic. (At this pressure the shock passage time should be only about 0.2 μ sec, which corresponds to 1 mm (one half of a subdivision) on the picture.)

In addition to a higher sensitivity, the film gauge shows one more interesting feature. As will be shown in the next section, the film gauge allows separation of variables by 3 simultaneous measurements which, in principle, can be carried out with one single filament.

C. Concerning Heat Transfer to a Film-Coated Probe.

It was pointed out above that for the intended measurements the filament necessarily operates in the free-molecule flow regime. The heat transfer in free-molecule flow has been treated by a number of authors (Refs. 6 - 10). According to reference 6 the heat transfer per unit surface area and time is

$$q = A\,\alpha \cdot \frac{\rho}{\rho_1}\left(\frac{T}{T_1}\right)^{3/2} \cdot f(s,\,\theta)\left[1 - \eta\,(s,\,\theta)\,\frac{T_s}{T}\right] \tag{11}$$

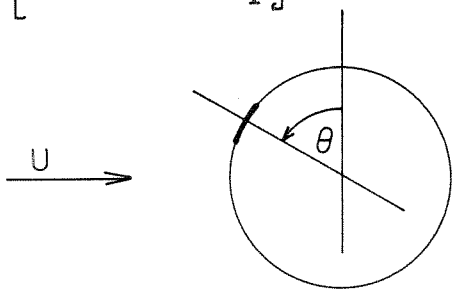

with

$A = \sqrt{\frac{2}{\pi\gamma}}\,p_1 a_1$

α = accommodation coefficient

T = static gas temperature

T_s = surface temperature of the filament

s = molecular speed ratio $s = \frac{U}{V_m}$

θ = orientation of the surface with respect to the flow direction.

$f(s,\theta)$ mainly represents the number density of the molecules impinging on the unit surface. It is easily seen that this is a strong function of both s and θ (mainly for moderate values of s as encountered in the shock tube). Consider a flat plate perpendicular to the flow direction. Under the assumption of free molecule flow the front side of the plate will be hit by all molecules except the ones with a negative velocity component (the velocity considered here is

the combined thermal and flow velocity). The rear side of the plate, however, is hit by molecules with negative velocity components only. With increasing flow velocity the number of molecules hitting the front side will increase and the number impinging on the rear side will decrease.

When the temperature is constant over the probe surface, equation 11 can be integrated over the circumference of the filament and gives

$$q = A\,\alpha\left(\frac{\rho}{\rho_1}\right)\left(\frac{T}{T_1}\right)^{3/2} F(s) \left[1 - H(s)\,\frac{T_s}{T}\right] \tag{12}$$

$f(s, \theta)$, $\eta(s, \theta)$, $F(s)$, $H(s)$ are given in the following table, which is computed for the case of a monatomic gas.

TABLE III

Numerical Values of $f(s, \theta)$, $\eta(s, \theta)$, $F(s)$ and $H(s)$

	$f(s, \theta)$				$\eta(s, \theta)$			
s	$\theta = \frac{\pi}{2}$	$\theta = 0$	$\theta = -\frac{\pi}{2}$	$F(s)$	$\theta = \frac{\pi}{2}$	$\theta = 0$	$\theta = -\frac{\pi}{2}$	$H(s)$
0	1.00	1.00	1.00	1.00	1.00	1.00	1.00	1.00
0.2	1.52	1.02	0.63	1.05	0.91	0.98	1.10	0.975
0.4	2.27	1.08	0.375	1.20	0.82	0.93	1.20	0.895
0.6	3.27	1.18	0.222	1.47	0.73	0.85	1.25	0.800
0.8	4.57	1.32	0.125	1.85	0.66	0.76	1.25	0.700
1.0	6.25	1.50	0.066	2.37	0.58	0.67	1.38	0.610
1.2	8.40	1.72	0.030	3.05	0.51	0.58	1.53	0.531
1.4	11.1	1.98	0.014	3.90	0.45	0.51	1.62	0.461

It is clear that the sensitivity of a partially-coated filament is strongly dependent on the orientation of the coated section with respect to the flow direction. The highest sensitivity is obtained when only a very thin band at the front stagnation line is coated.

Another result which may be the most important is the possibility of separation of the unknowns ρ, T, s using the θ-dependence of the functions $f(s, \theta)$ and $\eta(s, \theta)$. Consider 3 filaments partially coated and mounted with different orientation with respect to the flow direction ($\theta = \frac{\pi}{2}, 0, -\frac{\pi}{2}$).

The heat transfer is then

$$q_1 = A\, a \frac{\rho}{\rho_1} \left(\frac{T}{T_1}\right)^{3/2} f(s, \tfrac{\pi}{2}) \left[1 - \eta\,(s, \tfrac{\pi}{2})\, \frac{T_s}{T}\right]$$

$$q_2 = A\, a \frac{\rho}{\rho_1} \left(\frac{T}{T_1}\right)^{3/2} f(s, 0) \left[1 - \eta\,(s, 0)\, \frac{T_s}{T}\right] \qquad (13)$$

$$q_3 = A\, a \frac{\rho}{\rho_1} \left(\frac{T}{T_1}\right)^{3/2} f(s, -\tfrac{\pi}{2}) \left[1 - \eta\,(s, -\tfrac{\pi}{2})\, \frac{T_s}{T}\right]$$

Provided that q is known for each filament, equations 13 are sufficient to solve for ρ, T, S:

$$\frac{q_1}{q_2} = \frac{f(s, \frac{\pi}{2})}{f(s, 0)} \cdot \frac{\left[1 - \eta\,(s, \frac{\pi}{2})\, \frac{T_s}{T}\right]}{\left[1 - \eta\,(s, 0)\, \frac{T_s}{T}\right]}$$

As a first approximation (c.f. Table III)

$$\frac{1 - \eta\,(s, \frac{\pi}{2})\, \frac{T_s}{T}}{1 - \eta\,(s, 0) \frac{T_s}{T}} \doteq 1$$

so s is determined from

$$\frac{q_1}{q_2} = \frac{f(s, \frac{\pi}{2})}{f(s, 0)} \tag{14}$$

Figure 2 is a plot of $f(s, \frac{\pi}{2})/ f(s, 0)$. It is seen that this ratio is sensitive enough to changes in s, that s can be determined sufficiently accurately when $s \geq 0.3$. The existence of a lower limit for s, below which the method becomes useless, follows from the fact that the dependence of q on the orientation θ vanishes when the gas is at rest ($s = 0$). Once s is known, ρ, T can be obtained from equation 13.

This method requires the knowledge of q at each instant; q can be calculated from (Ref. 11, p. 133)

$$q(t) = \sqrt{\frac{k \rho c}{\pi}} \left[\frac{T(t_0)}{t} + \int_0^t \frac{T'(t - \tau)}{\sqrt{\tau}} \, d\tau \right] \tag{15}$$

This formula was written in a different form by R. J. Vidal (Ref. 12) in order to avoid the troublesome derivative. G. T. Skinner (Ref. 13) has developed an analog network to obtain q from the time history of the probe. Work in this direction has not been undertaken in this investigation since the first experiments (described in Section IV) indicate that the signal produced by the present configuration of the probe is too small to permit quantitative analysis of the shock structure. However a few probes were constructed with a filament which had a very narrow film along the stagnation line and a very

definite increase in sensitivity was obtained.

Figure 1.b shows the output obtained from a filament, which was oriented in such a way that the coated section was directed away from the incident shock. This results in a small signal caused by the incident shock and a much larger signal obtained from the reflected wave. Typical traces for properly oriented filaments are shown in figure 8.

III. DESCRIPTION OF THE PROBE

The construction of the filament probe is similar to the construction of a cold wire or hot wire probe except that the sensitive element is now a filament of non-conducting material, coated with a thin film of conducting material. In this section some details of the probe and its construction will be discussed.

A. Filament.

All filaments used in this work were drawn from either quartz or Pyrex rods 3 mm in diameter. Those materials were chosen for a number of reasons: ready availability, high softening temperatures*, high tensile strength and favorable thermal properties. Although some synthetic fibers have thermal properties much better than those of quartz or Pyrex, no attempt was made to use those fibers since they have a low softening temperature and poor strength. The Pyrex filaments had the advantage of being more flexible than the quartz filaments. It was also found that the breakage of the filaments in the shock tube was lower with Pyrex than with quartz.

The cross section of many of the drawn filaments was checked under a microscope and was found to be very circular. The filament diameter is largely determined by the conditions for free-molecule flow over the probe and one-dimensional heat conduction in the filament. According to references 6 and 7 free-molecule flow exists over the filament when

$$\frac{\Lambda}{d} \geqslant 2 - 5 \qquad (16)$$

* This is considered an important property since during the coating process the filament heats up considerably due to its high l/d ratio and intense radiation emitted from the tungsten coil (c.f. below).

With Argon at 50 μHg as test gas and assuming $\frac{\rho_2}{\rho_1} = 4$ across the shock, equation 16 yields $D \leq 5$ mil as an upper limit for the filament diameter. A lower limit for the diameter is obtained from the condition for one-dimensional heat flux in a semi-infinite body. (See Section II.a, Eq. 10a.) This yields

$$D > \sqrt{2.5\,\tau_{max}} \tag{17}$$

With $\tau_{max} = 6$ μsec (shock passage time over a fixed point) equation 17 gives $D \geq 4$ mil. The diameter of the filaments was therefore taken between 4 and 5 mils.

After the filaments were drawn they were cut to approximately 3" lengths, thoroughly cleaned and put on a 2" x 3" frame which held about 30 filaments. They were then coated simultaneously by the vacuum evaporation technique (Ref. 14). Wire made of the metal to be evaporated was wound on a 3" long by 1" diameter spiral of braided tungsten wire. Very good reproducibility of the film thickness was obtained by monitoring the electrical resistance of a dummy gauge during the coating process. Metals evaporated are listed below:

a) Chromium adhered very well to quartz or Pyrex but did not give a reproducible temperature coefficient of resistivity.

b) Nickel did not adhere to Pyrex or quartz.

c) Platinum gave by far the best results and was used for all final filaments.

Some trouble was encountered in an attempt to improve the

properties of the films by baking the freshly coated filaments in an electric oven at 500° C (Ref. 15). Better results were obtained by aging the film under vacuum by means of an electric current. The procedure was as follows: The probes were made with unbaked filaments and were then placed in a vacuum chamber at 1 μ Hg. The filament formed one arm of a Wheatstone bridge through which a relatively high current (typically 30 mA) was sent for about 15 minutes. In this way the resistance of the film could be measured continuously. In a typical case the resistance would initially rise (due to Joule heating) to about 175 per cent of the initial cold resistance and would then gradually decrease (due to aging) to about 150 per cent after which the resistance remained very stable.

The final cold resistance of most probes was around 400 Ω. (Knowing the length and the diameter of the filament, and assuming the bulk coefficient for the electrical resistivity ($\sigma \doteq 10^{-5}$ ohm. cm) the effective film thickness was found to be approximately 200 Å.)

B. Construction of the Probe.

The construction of the probe is illustrated in figure 3, which is a partial cutaway view of the probe mounted in the end wall of the 17-inch shock tube. A good vacuum seal was obtained by means of Kovar-glass tubular lead-through's. Soft solder joints were used everywhere. For measurements of shock reflection from the end wall it was very important that the end wall near the probe be kept plane, so as not to introduce disturbances which might influence the reflection process. For that reason the holes in which the Kovar-glass seals were mounted, were filled flush with epoxy. The

shoulder on the brass plug which carried the probe, was machined so that the plug face would be flush with the end wall to an accuracy of $\pm$ .001". The volume of gas between the brass plug and the hole in the end wall was minimized by machining the diameter of the plug to within .001" of the diameter of the hole in the end plate.

The filaments were supported by a .025" diameter drill rod. For the first series of measurements two filaments were attached to the supports, one at the tip of the "needles" about 1 inch from the end wall and the other about $\frac{1}{2}$ inch from the base. In order to facilitate the replacement of broken filaments the supports were grooved after they had been soldered to the Kovar-glass seals. (This was the main reason for choosing drill rod for the supports rather than conventional needles.) This proved to be extremely useful. Although the filaments withstood the conditions in the shock tube better than expected, frequent replacement of the filaments was necessary. Thanks to the grooves the replaced filament was always parallel with the front face of the brass plug and it was found that in this way the distance from the end wall could be repeated to within .001".

The filaments were glued to the supports. Various kinds of epoxy were tried* and the best results were obtained from Miracle Adhesive No. 185, which sets at room temperature. Application of heat which was found to cause sagging of the filaments was thereby avoided. The epoxy was allowed to cure for about 15-20 hours. The

* At a certain point a conductive cement (Eccobond 58c) was tried in order to reduce contact noise to a minimum. This cement has the advantage of curing at low temperatures but insufficient mechanical strength results.

electrical connection between the film on the filament and the supports was then made by means of silver print (Walsco-36). The film was then aged electrically as described above.

The distance between the filaments and the front face of the brass plug was measured on an optical comparator (Kodak Contour Projector, Model 2A) with a 50x magnification and could be measured to better than .001". It is worth noting that for shock reflection measurements in Argon with $M_s = 4.0$ a 1 mil uncertainty in the location of the filament introduces an error of .05 μ sec into the measured time interval (i.e., the time between the passage of the incident shock and the reflected shock over the same filament).

IV. REFLECTED SHOCK MEASUREMENTS

A. Introduction.

Certain properties of reflecting shock waves have recently been investigated by a number of authors (Refs. 16 - 22). This interest was prompted by the extensive use of the region behind the reflected shock as a test region for chemical reactions and the associated need to know the thermodynamic conditions and their uniformity in this region. In the references cited the reflected shock speed in various gases has been studied over wide ranges of initial pressure and incident shock Mach number. Although the details of their findings do not always agree the common results can be summarized as follows.

In most gases (He and A excepted) the interaction of the reflected shock and the boundary layer in the flow behind the incident shock leads to shock bifurcation (Ref. 19) and boundary layer separation behind the reflected shock. Cohen and Strehlow (Refs. 17-18) studied the growth of the bifurcation legs and related the measured deceleration and subsequent acceleration of the reflected shock to this growth. Particularly striking x-t pictures can be found in reference 18. All experimenters agree on the fact that no shock bifurcation is found in the case of Argon or Helium. Mark (Ref. 19) relates this to the higher value of γ for He and A. Furthermore the measured speed of the reflected shock in Argon is found to be lower than the speed predicted by the inviscid theory. It should be noted that most measurements of the reflected shock speed extend over several tube diameters from the end wall and therefore, the effect of the side walls on the measured shock speed can be expected to be important. The purpose

of this work is to study the shock reflection for conditions which approach as closely as possible the reflection of a plane shock from an infinite wall. There is little doubt that the influence of the side walls of the tube on the center portion of the reflected shock wave remains completely negligible while the shock wave is less than about $\frac{1}{10}$ of the tube diameter from the end wall.

In the 17-inch shock tube this condition leaves a cylindrical region of about 2" depth which is free of side wall influence and hence is useful for measuring the reflected shock speed. This is illustrated in figure 4, showing the location of the probes and the instantaneous positions of the center portion of the reflected shock wave and of a sound wave emitted from the side wall at the instant of arrival of the incident shock wave at the end wall. The relative positions are shown at two instants, corresponding to the time when the reflected shock wave is at distances of 1" and 2" from the end wall ($M_s = 4.0$ is assumed).

B. On the Reflection of a Normal Shock Wave from a Plane Heat Conducting End Wall.

When all effects of heat transfer to the end wall are neglected, the velocity of the reflected shock ($u_{R,I}$) is obtained from the condition $u_5 = 0$ (Ref. 23). For the case of a perfect gas the expression for the reflected shock speed can be reduced to the following simple form:

$$\frac{u_{R,I}}{u_s} = \frac{2(\gamma - 1) M_s^2 - (\gamma - 3)}{(\gamma + 1) M_s^2} \tag{18}$$

($u_{R,I}$, u_s in lab fixed coordinates).

A qualitative estimate of the influence of the heat transfer to the end wall on the reflected shock can be obtained from the following simple model. It is well known that, even for moderately strong shocks, the temperature T_5 of the gas behind the reflected shock is much higher than the initial gas temperature T_1 (for most practical applications T_1 = temperature of the shock tube walls). Hence, as soon as the shock reflects, a layer of hot gas adjacent to the cool end wall will be formed. Heat will then flow from the gas to the wall and the temperature at the interface between gas and wall will jump to

$$T_i = \frac{\beta_w}{\beta_w + \beta_5} T_1 + \frac{\beta_5}{\beta_w + \beta_5} T_5$$

with $\beta = \sqrt{k \rho c}$

Since $\beta_w \gg \beta_5$, the interface temperature will not differ much

from the initial wall temperature.

A cool layer will then develop in the gas adjacent to the end wall. An effective thickness δ_5 of the thermal layer in the gas can be defined by

$$\delta_5 (T_5 - T_1) = \int_0^\infty (T_5 - T)\, dx$$

It is easily found that δ_5 grows like $\sqrt{\frac{k_5 t}{\rho_5 c_p}}$ or $\delta_5 \sim \sqrt{\nu_5 t}$ Due to the high density in the cool layer, mass will accumulate in this layer. This will cause a flow toward the end wall in the region behind the reflected shock. The flow velocity v' toward the end wall is clearly proportional to the growth rate of the cool layer on the end wall(cf. Fig. 5).

$$v' \sim v = \frac{d\delta_5}{dt} \sim \sqrt{\frac{\nu_5}{\tau}}$$

The reflected shock wave is no longer determined by the condition $u_5 = 0$ but by $u_5 = v'$ and thus the velocity jump across the reflected shock is now reduced to $\Delta u = u_2 - v'$. This leads to a weaker (and thus slower) reflected shock wave than is predicted by the ideal theory. Since v decreases with increasing time, one would expect the reflected shock to accelerate and asymptotically reach the velocity predicted by the ideal theory.

One can look at the mass defect into the cool layer as if it were caused by a receding end wall. This is illustrated in figure 6. The dotted line represents the fictitious displacement of the end wall.

The initial infinite velocity* produces an expansion wave which cancels the incident shock wave. During the subsequent deceleration of the end wall compression waves are emitted which converge to form the reflected shock wave. The compression waves accelerate the reflected shock toward its ideal velocity. A quantative treatment of this phenomenon carried out by Goldsworthy (Ref. 24) results in

$$u_R = u_{R,\,I} - f(M_s)\ \frac{1}{1+m}\sqrt{\frac{k_5}{\rho_5 c_p \pi t}} \tag{19}$$

with

$$m^2 = \frac{k_5 \rho_5 c_p}{k_w \rho_w c_w} = \frac{\beta^2_5}{\beta^2_w} \ll 1$$

Or upon integration

$$x_R = x_{R,\,I} - 2\, f(M_s)\ \sqrt{\frac{k_5 t}{\rho_5 c_p \pi}} \tag{20}$$

Defining $x^* = \frac{x}{\Lambda_2}$ and $t^* = \frac{t}{\tau}$ with Λ_2 = mean free path in region 2 and $\tau = \Lambda_2 / u_{R,I}$

one obtains

$$x^*_R = x^*_{R,\,I} - g(M_s)\sqrt{\frac{k_2 t}{\rho_2 \Lambda_2 c_p \pi}} \tag{21}$$

* The singularity at t = 0, i.e., small Reynolds number, is typical of boundary layer calculations and reflects the inapplicability of the boundary layer approximation at small times.

where

$$g(M_s) = 2 f(M_s) \sqrt{\frac{\left(\frac{T_5}{T_2}\right)^{\omega} \frac{\rho_2}{\rho_5}}{u_{R,\,I}}}$$

To obtain the last relation it has been assumed that the temperature behavior of conductivity has the form $k \sim T^{\omega}$. $g(M_s)$ is found to be a slowly varying function of M_s. Equation 21 clearly indicates that the non-dimensional reflection curve is independent of the initial pressure but depends on both M_s and T_1. This property will be used in the reduction of the experimental data.

C. Experimental Arrangement.

a) Shock Tube.

A description of the 17-inch GALCIT shock tube in which the experiments were carried out, can be found in reference 1 and additional operational information is given in reference 25. One major alteration has been made in the 17-inch shock tube since the above mentioned descriptions. The adjustable knife blades, as described in references 1, 25 and 26, were replaced by an interchangeable set of 3 fixed knife blades with different radii of curvature, and plates which changed the tube cross-section from circular to nearly square, were installed at the diaphragm station. The purpose of these changes was to enable the use of a wider variety of diaphragm materials and thicknesses, and consequently to extend the range of obtainable shock speeds, which had previously been limited by loss of petals from the ruptured diaphragms. The bursting pressures obtainable with soft aluminum diaphragms ranging in thickness from .006" to .020", now start from as low as 9 psia and go up in steps of 15-20 per cent to about 40 psia. In this way and with the use of mixed driver gases (Ref. 25) any Mach number from 3.5 to 8 can be obtained in Argon.

b) Experimental Equipment and Data Recording Procedure.

The time history of the reflected shock wave was measured using filament probes (Fig. 3) with needles of various lengths. For each run three probes were flush mounted in the stainless steel end plate of the 17-inch shock tube (Fig. 4). The maximum distance between the filaments and the end wall did not exceed 1 inch, whereas

the minimum distance between filament and side wall was 5 inches. It is therefore felt that no disturbances caused by the reflected shock wave-boundary layer interaction have influenced the measurements.

From the recorded output of each filament the passage of the incident and reflected shock wave could then be determined. The accuracy with which this could be done was greatly helped by the parabolic behavior of the signal output of the film gauge. In order to obtain equal sensitivity for both the incident and the reflected shock, care was taken to mount the filaments on the needles such that the film formed an angle $\theta = 0$ with the direction of propagation of the shock wave (cf. Section II.C). Figure 1.b clearly shows the influence of the orientation of the film.

The data were recorded in the usual way, i.e., the probe output was displayed on oscilloscopes and recorded on Polaroid Type 47 film. In order to obtain good timing accuracy from the traces, the sweep speed of the oscilloscopes was kept as high as possible by displaying the output of one probe over two successive oscilloscope traces. For three probes a total number of six beams was thus required. They were supplied by three dual-beam Tektronix oscilloscopes. (Two 555-scopes and one 551-scope.) Figure 7 is a block diagram of the system. The output of the probes was preamplified (this was omitted at higher pressures) and then fed to the vertical deflection amplifiers of the oscilloscopes. All oscilloscopes were set for single sweep operation.

The six available beams were triggered in two successive groups of three beams each. The triggering signal was obtained from

a side wall film gauge mounted 200 mm upstream of the end plate. The signal from this gauge was used to start a delay generator. This unit fired a trigger pulse after a preset time (typically 130 μ sec.). This trigger pulse was used to start sweep generators for the first group of three beams and also to start a second delay generator, which, after a preset delay time (varying from 12 to 45 μ sec.), triggered the second group of three beams.

Matching the two consecutive traces of one probe was achieved by means of Z-modulation of all traces. This was accomplished by presenting the output of a square-pulse generator (Dumont type 404) to the C.R.T. cathodes. The generator was adjusted for a frequency of 100 Kc, a pulse width of 0.4 - 0.7 μ sec. and an amplitude of 30 volts. As a result all traces showed synchronous "black spots". Figure 8 shows a typical set of traces obtained for each shot. Note that the output of probe No. 1 is displayed on beams 1 and 4; probe No. 2 is shown on beams 2 and 5, etc. The frequency of the pulse generator was recorded with each run by a microsecond counter (Beckman-Berkeley model 7370) on the E/UT function. As a fringe benefit calibration of the sweep speed of the oscilloscopes was made possible using the time markers in the traces. A certain non-linearity in the sweep speed was detected but it was too small to be accounted for.

The shock speed was recorded at two stations in the shock tube, located approximately 1 and 10 diameters upstream of the end plate. A 1 per cent deceleration was usually measured between the two stations ($\doteq$ .1 per cent per foot).

c) Range Covered by Experiments.

It can be seen from equation 20 that the parameters governing the motion of the reflected shock wave in a particular gas are: p_1, T_1 and M_s. Of those three parameters only p_1 was varied. Three pressure levels were used: p_1 = 50, 100 and 500 μ Hg. The Mach number of the incident shock, M_s, was held nearly constant and equal to 4.08 ($\pm$ 2 per cent) by changing the diaphragm thickness and using mixed driver gases. Argon was used as test gas for all experiments.

The displacement-time relation for the reflected shock wave was measured with six different probe assemblies, each one of which had provision for mounting the filament at two different locations. The resulting twelve measurement stations covered the region from .100" to .950" from the end wall in steps of approximately .075". As mentioned above, the mean free path in region 2, Λ_2, was used as a reference length with respect to which the filament location (x) was non-dimensionalized ($x^* = x/\Lambda_2$). The range of x^* covered in this work extends from 8 to 800.

The experiments were carried out in five series of runs which differed by either the initial pressure, p_1, and/or the range of distances from the end wall covered by the filaments.

Series 1 : p_1 = 100 μ Hg, 2 filaments/probe $16 < x^* < 160$

Series 2 : p_1 = 100 μ Hg, 1 filament/probe $17 < x^* < 81$

Series 3 : p_1 = 50 μ Hg, 1 filament/probe $8.3 < x^* < 40.5$

Series 4 : p_1 = 50 μ Hg, 1 filament/probe $54 < x^* < 79$

Series 5 : p_1 = 500 μ Hg, 1 filament/probe $210 < x^* < 800$

D. Data Reduction.

The traces recorded with each run were reduced to give the time of arrival of both the incident and the reflected shock wave at the different filament locations. The arrival of either wave is determined as the intersection of the tangents to the trace before and after arrival of the wave. The two successive traces of the output of one probe were matched by means of the synchronous time markers in the traces and $(t_r - t_i)$, the time elapsed between the arrival of the incident and reflected wave at a filament, was then easily obtained. The time of impact $(t_o - t_i)$ of the incident shock on the end wall was computed for each filament separately using the time of arrival of the wave at the filament as well as the velocity of the shock wave (u_s), as measured between two side wall gauges mounted 700 and 200 mm upstream of the end wall. Finally $(t_r - t_o)$, the time used to plot the x, t diagram of the reflected shock wave, was obtained by subtraction.

x and $(t_r - t_o)$ were non-dimensionalized with the mean free path and reflected shock velocity; $x^* = \frac{x}{\Lambda_2}$ and $t^* = \frac{(t_r - t_o)}{\Lambda_2 / u_{R,I}}$. Λ_2 and $u_{R,I}$ (Eq. 18) were calculated for each run separately in order to account for the slight variations of M_s.

For the dimensional x, t diagram slight variations of M_s were accounted for using the following correction formula, which is derived from equation 18:

$$\frac{d\,(t_r - t_o)}{(t_r - t_o)} = \left[\frac{2(\gamma - 1)\,M_s^2 - (3 - \gamma)}{2(\gamma - 1)\,M_s^2 + (3 - \gamma)}\;\frac{d\,M_s}{M_s}\right]$$

Table IV presents the actual reduction of the traces shown in figure 8a.

TABLE IV

Data Reduction for Figure 8a

$p_1 = 50\ \mu$ Hg

$a_1 = 322$ m/sec

$M_s = 4.16$

Sweep speed: 5 μ sec/cm

Pulse frequency: 99.9×10^3 cps.

Vertical deflection: 2 mV/cm

$\frac{1}{\Lambda_2} = 3.35\ \text{mm}^{-1}$, $\frac{u_{R,I}}{\Lambda_2} = 2.37\ \mu\text{sec}^{-1}$

$(t_r - t_o)_{corr.} = 1.011\,(t_r - t_o)$

Instrumentation:

Probe No. 1 displayed on beams 1 and 4

Probe No. 2 " " " 2 and 5

Probe No. 3 " " " 3 and 6

Probe	x (mm)	$t_r - t_i$ (μ sec)	$t_o - t_i$ (μ sec)	$t_r - t_o$ (μ sec)	t*	x*	$(t_r - t_o)_{corr.}$ (μ sec)
No. 1	23.72	60.07	17.70	42.37	100.5	79.4	42.84
No. 2	19.01	49.35	14.20	35.15	83.4	63.6	35.54
No. 3	16.01	42.47	12.15	30.32	71.9	54.2	30.65

E. Results.

The measured x, t diagrams of the reflected shock wave are shown in figures 9, 10 and 11 with the straight line corresponding to the ideal shock reflection and the curve predicted by the theory*. Figure 9 is a dimensional plot, whereas figures 10 and 11 are non-dimensional x, t diagrams, the former being a logarithmic plot of all the data and the latter a linear plot near the wall. It is shown above (Eq. 21) that in non-dimensional form the theoretical curve is independent of the initial pressure, but remains dependent on k_5, the thermal conductivity in region 5. Figure 11 shows the theoretical curve for two different values of k_5 one value ($k_5 = 2.45 \times 10^{-4}$ cal/cm sec ^{o}K) is computed from the Lennard-Jones potential (Ref. 27) whereas the other value ($k_5 = 2.80 \times 10^{-4}$) is taken from reference 28. The latter value is based on beam scattering experiments. Those values of k yield:

$$x^* = t^* - 2.03\sqrt{t^*} \quad (k = 2.80 \times 10^{-4})$$

and

$$x^* = t^* - 1.89\sqrt{t^*} \quad (k = 2.45 \times 10^{-4})$$

At large distances ($x^* \geq 70$) the agreement between the theory and the measurements is striking and, in this region, a very good approximation to the actual speed of the reflected wave is obtained from the theory. At $x^* = 100$ the shock is approximately 10 per cent slower than the ideal reflected shock and at $x^* = 900$ there is only a 3 per cent discrepancy between the ideal and the actual velocity.

* Whenever reference is made to the theory it is understood that this is the theory of the reflected shock as given by Goldsworthy in reference 24.

Extending this into the region farther away from the end wall than the one covered by the experiments one finds that the reflected shock speed is within 1 per cent of the ideal speed for $x^* = 10^4$, provided the interaction between the reflected shock wave and the side-wall boundary layer has not yet perturbed the flow. At very low pressures(p_1 = 100 μHg) it is expected that the boundary layer interaction will play an important role long before the reflected shock reaches this 1 per cent mark (e.g., at p_1 = 100 μHg $x^* = 10^4$ corresponds to $x = 1.5 \times 10^3$ mm, which is very large compared to the diameter of existing shock tubes). At higher pressures however (e.g., p_1 = 1 cm Hg, $x^* = 10^4$ corresponds to x = 15 mm) it is quite possible that in this case, even in a medium sized shock tube, the reflected wave will accelerate to a speed, very close to the ideal speed, before the boundary layer interaction becomes important. It is possible that the different combinations of initial pressure and tube diameters used by different experimentors are responsible for the observed differences in reflected wave speeds. It is felt that these conclusions are largely independent of M_s since the coefficient a in the equation $x^* = t^* - a\sqrt{t^*}$ is only a weak function of M_s.

The temperature directly behind the reflected shock wave can easily be calculated once the speed of propagation of the reflected wave is known. It turns out that when the reflected shock is about 100 mean free paths from the end wall the temperature right behind the reflected shock is approximately 5 per cent below the ideal temperature T_5. This difference decreases rapidly when the reflected wave moves farther away from the end wall. It is obvious that due to the acceleration

of the reflected shock on one hand and the growth of the cool layer on the other hand the temperature in region 5 will be highly non-uniform as long as the shock wave is within a few hundred mean free paths from the end wall. At very low initial pressures this might exclude the use of region 5 for chemical reaction experiments.

Closer to the end wall ($x^* \leqslant 70$) the measurements start deviating from the theory. This is to be expected since the theory is of the boundary layer approximation type and is clearly restricted to large Reynolds numbers (or x^*, in this case). It is interesting to note that the theory which actually is an approximation for large x^* is valid for x^* as low as 70. It is also worth noting that the theory predicts a shock wave, which initially disappears into the end wall and emerges from it after a finite time interval (Fig. 11). This is physically impossible and, even when the theory adequately describes the motion of the reflected shock far away from the end wall, one should expect the measured points to fall below the theoretical curve. This is in fact observed (Fig. 11).

The closest measurement point was located at 8 mean free paths (measured in region 2) from the end wall. A filament located at this distance from the end wall will still be submerged in the tail of the incident shock when the tip of the shock has already reached the end wall and starts reflecting from this wall. The microscopic details of the reflection of a shock involve molecular processes, and the formation distance of the reflected shock wave is of the order of a few mean free paths. The speed of the reflected shock wave as it emerges from its formation region is related to the accommodation coefficient

for the particular combination of gas and wall. Accurate measurements of the velocity with which the reflected shock wave emerges from its formation region might shed some light on processes of accommodation.

Far away from the end wall ($x^* > 70$) it is seen that the motion of the reflected shock is governed by the heat diffusion in the gas in region 5, and from measurements in this region it is possible in principle, to derive the coefficient of thermal conductivity in region 5.

V. CONCLUSIONS

There is little doubt that the filament probe is a useful instrument with which to carry out accurate timing in low pressure shock tube experiments. Further improvements might make it sensitive enough to allow some quantitative analysis of the structure of thick moving shock waves.

The measurements of the reflected shock wave indicate the existence of three different regions near the end wall:

a) The region close to the end wall where the reflected shock forms ($x^* \lesssim 10$). Here the assumption of a continuum breaks down and the phenomenon is governed by molecular processes. Much might be learned about processes of accommodation from an accurate knowledge of the velocity with which the reflected shock wave emerges from its formation region and propagates into the transition region.

b) The transition region ($10 \lesssim x^* \lesssim 70$). In this region the assumption of continuum is valid, but the boundary layer approximation does not apply.

c) The region far away from the end wall ($x^* \gtrsim 70$). It is shown that in this region the reflected shock theory applies and actually offers a possibility of obtaining experimental information about the thermal conductivity of gases at high temperatures. It is a very interesting result that the boundary layer approximation becomes valid for values of the Reynolds number as low as 70.

REFERENCES

1. Liepmann, H. W., Roshko, A., Coles, D., and Sturtevant, B.: A 17-Inch Diameter Shock Tube for Studies in Rarefied Gas-dynamics. Rev. Scientific Instruments, 33, No. 6, 625-631, June 1962.

2. Christiansen, W. H.: Development and Calibration of a Cold Wire Probe for Use in Shock Tubes. GALCIT Hypersonic Research Project Memo No. 62, July 1, 1961.

3. Vidal, R. J.: Transient Surface Temperature Measurements. Cornell Aero. Lab. Rep. No. 114, March 1962.

4. Hall, J. G., and Hertzberg, A.: Recent Advances in Transient Surface Temperature Thermometry. Jet Propulsion-American Rocket Society Journal, 28, 719-722, November 1958.

5. Carslaw, H. S., and Jaeger, J. C.: Conduction of Heat in Solids. Clarendon Press, Oxford, 1947.

6. Stalder, J. R., Goodwin, G., and Creager, M.O.: A Comparison of Theory and Experiment for High-Speed Free-Molecule Flow. NACA TN 2244, December 1950.

7. Cybulski, R. J., and Baldwin, L. V.: Heat Transfer from Cylinders in Transition from Slip Flow to Free-Molecule Flow. NASA Memo 4-27-59E, 1959.

8. Nocilla, S.: On the Interaction between Stream and Body in a Free-Molecule Flow. Laboratory of Applied Mechanics, Politechn. Inst. of Torino, July 1956.

9. Stalder, J. R., and Jukoff, D.: Heat Transfer to Bodies Traveling at High Speed in the Upper Atmosphere. NACA TN 1682, August 1948.

10. Schaaf, S. A., and Chambre, P. L.: Flow of Rarefied Gases. High Speed Aerodynamics and Jet Propulsion, Vol. III, Section 11. Princeton Univ. Press, 1958.

11. Churchill, R. V.: Operational Mathematics. McGraw Hill, 1958.

12. Vidal, R. J.: Model Instrumentation Techniques for Heat Transfer and Force Measurements in a Hypersonic Shock Tunnel, WADC TN 56-315, February 1956.

13. Skinner, G. T.: Analog Network to Convert Surface Temperature to the Heat Flux. Cornell Aero. Lab. Rep. 100, February 1960.

14. Holland, L.: Vacuum Deposition of Thin Films. Wiley, 1956.

15. Belser R. B.: Electrical Resistance of Thin Metal Films before and after Artificial Aging by Heating. J. Appl. Physics, 28, 109-116, 1957.

16. Toennies, J. P., and Greene, P. F.: Dissociation Energies of Carbon Monoxide and Nitrogen from Reflected Shock Wave Studies. J. Chem. Physics, 26, 655-662, 1957.

17. Strehlow, R. A., and Cohen, A.: Comment on Reflected Shock Wave Studies. J. Chem. Physics, 28, 983-985, 1958.

18. Strehlow, R. A. and Cohen, A.: Limitations of the Reflected Shock Technique for Studying Fast Chamical Reactions and its Application to the Observation of Relaxation in N_2 and O_2. J. Chem. Physics, 30, 257-265, 1959.

19. Mark, H.: The Interaction of a Reflected Shock Wave with the Boundary Layer in a Shock Tube. Cornell Univ. AFOSR TN-57-345, June 1957.

20. Mark, H.: The Interaction of a Reflected Shock Wave with the Boundary Layer in a Shock Tube. J. Aero. Sciences, 24, 304-306, April 1957.

21. Byron, S., and Rott, N.: On the Interaction of the Reflected Shock Wave with the Laminar Boundary Layer on the Shock Tube Walls. Proc. 1961 Heat Transfer and Fluid Mechanics Institute.

22. Wilkerson, T.: The Use of the Shock Tube as a Spectroscopic Source with an Application to the Measurement of gf-Values for Lines of Neutral and Singly Ionized Chromium. Technical Note, University of Michigan, June 1961.

23. Glass, I. I., and Hall, G. J.: Handbook of Supersonic Aerodynamics, Section 18, Shock Tubes. NAVORD Rep. 1488 (Vol. 6) December 1959.

24. Goldsworthy, F. A.: The Structure of a Contact Region, with Application to the Reflection of a Shock from a Heat-Conducting Wall. J. Fluid Mech. 5, 164-176, 1959

25. Johnson, D. S.: Design and Application of Piezoceramic Transducers to Transient Pressure Measurements. Thesis, Calif. Inst. of Technology, June 1962.

26. Roshko, A. and Baganoff, D.: A Novel Device for Bursting Shock-Tube Diaphragms. Phys. Fluids, 4, 1445, 1961.

27. Hirschfelder, J.O., Curtiss, C.F., and Bird, R.B.: Molecular Theory of Gases and Liquids. Wiley, 1954.

28. Amdur, I., and Mason, E.A.: Properties of Gases at Very High Temperatures. Phys. Fluids, 1, 370-393, 1958.

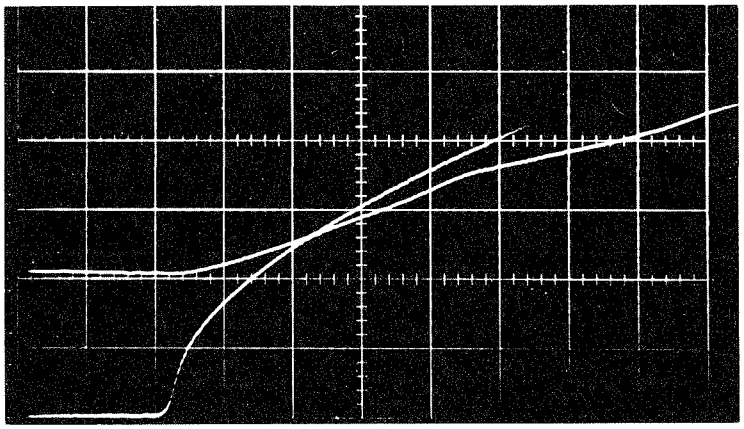

Fig. 1a. Comparison of the Responses of a .01 mil Wire and a Pt-coated Filament. Sweep speed 2 μsec/cm, vertical deflection 10 mv/cm.

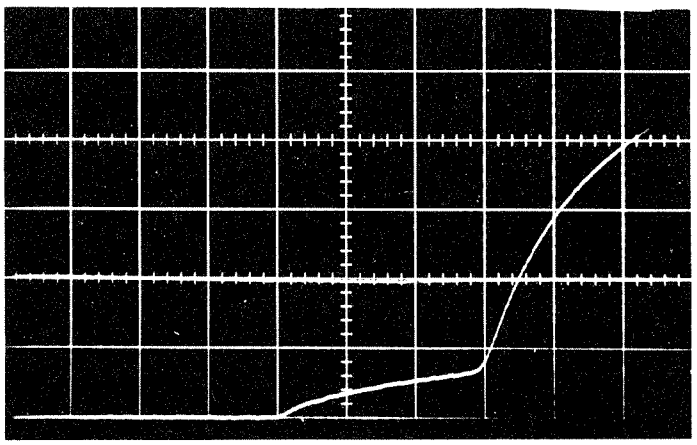

Fig. 1.b. Response of an Improperly Oriented Filament.

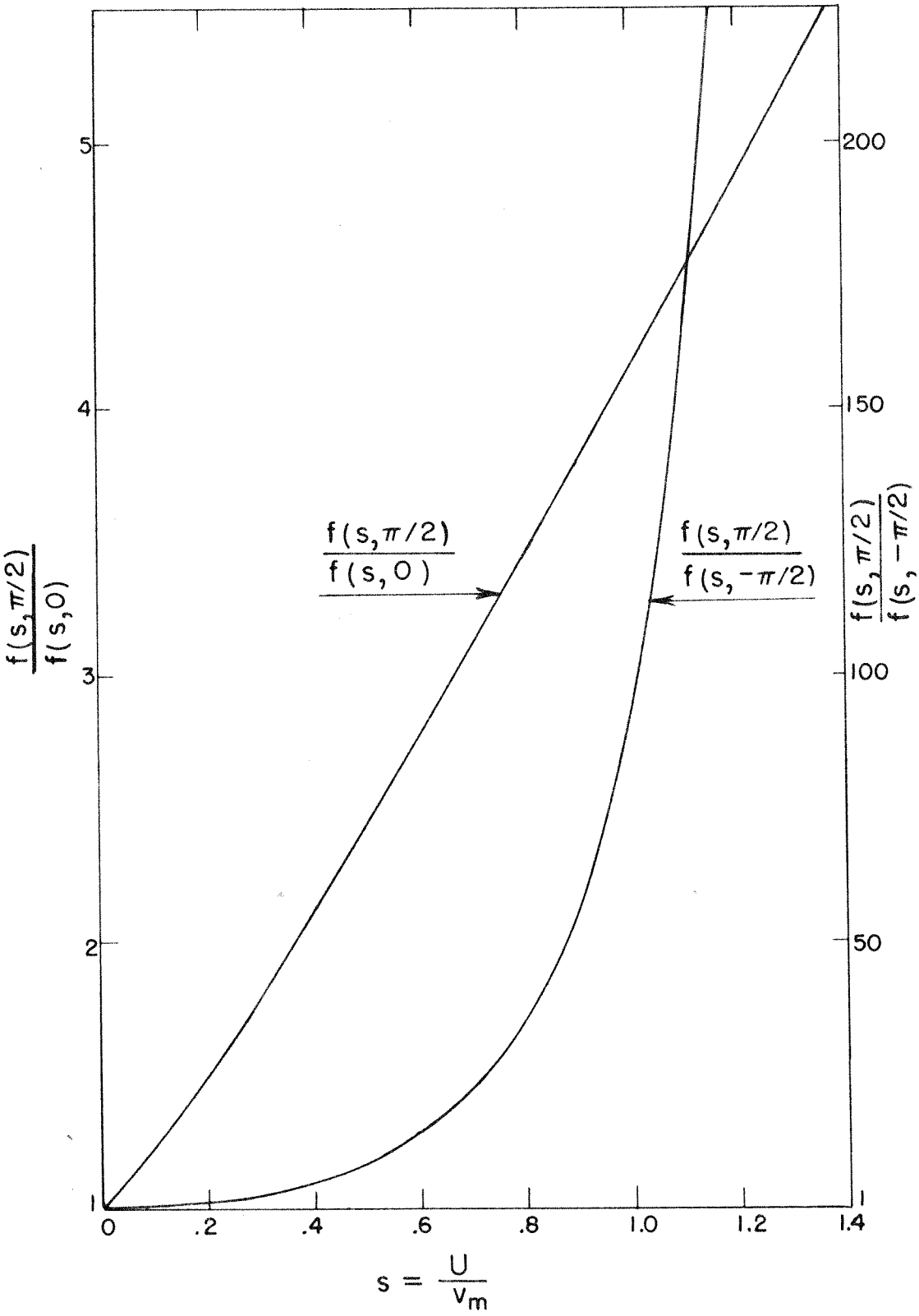

Fig. 2. Influence of Orientation Angle θ on Heat Flux.

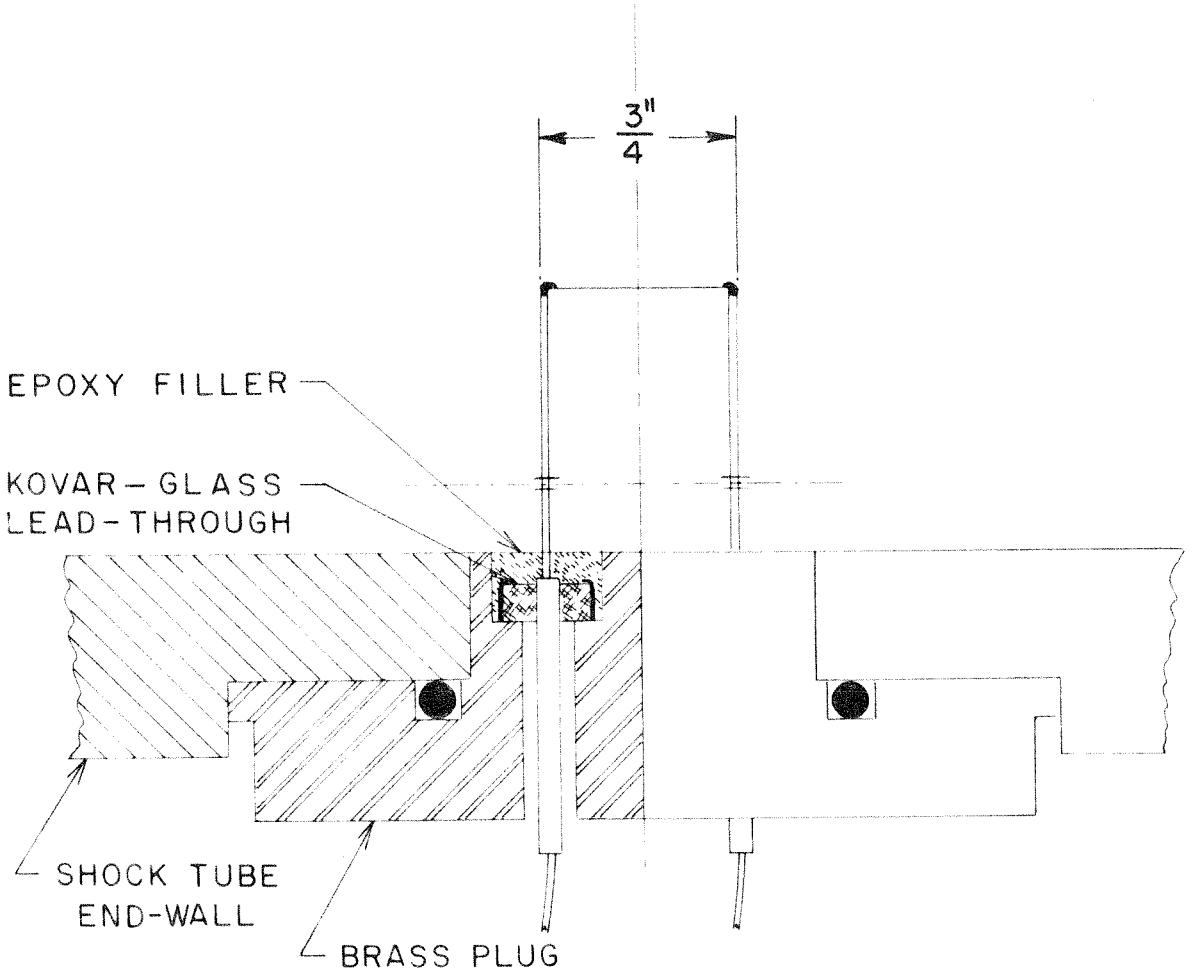

Fig. 3. Probe Construction.

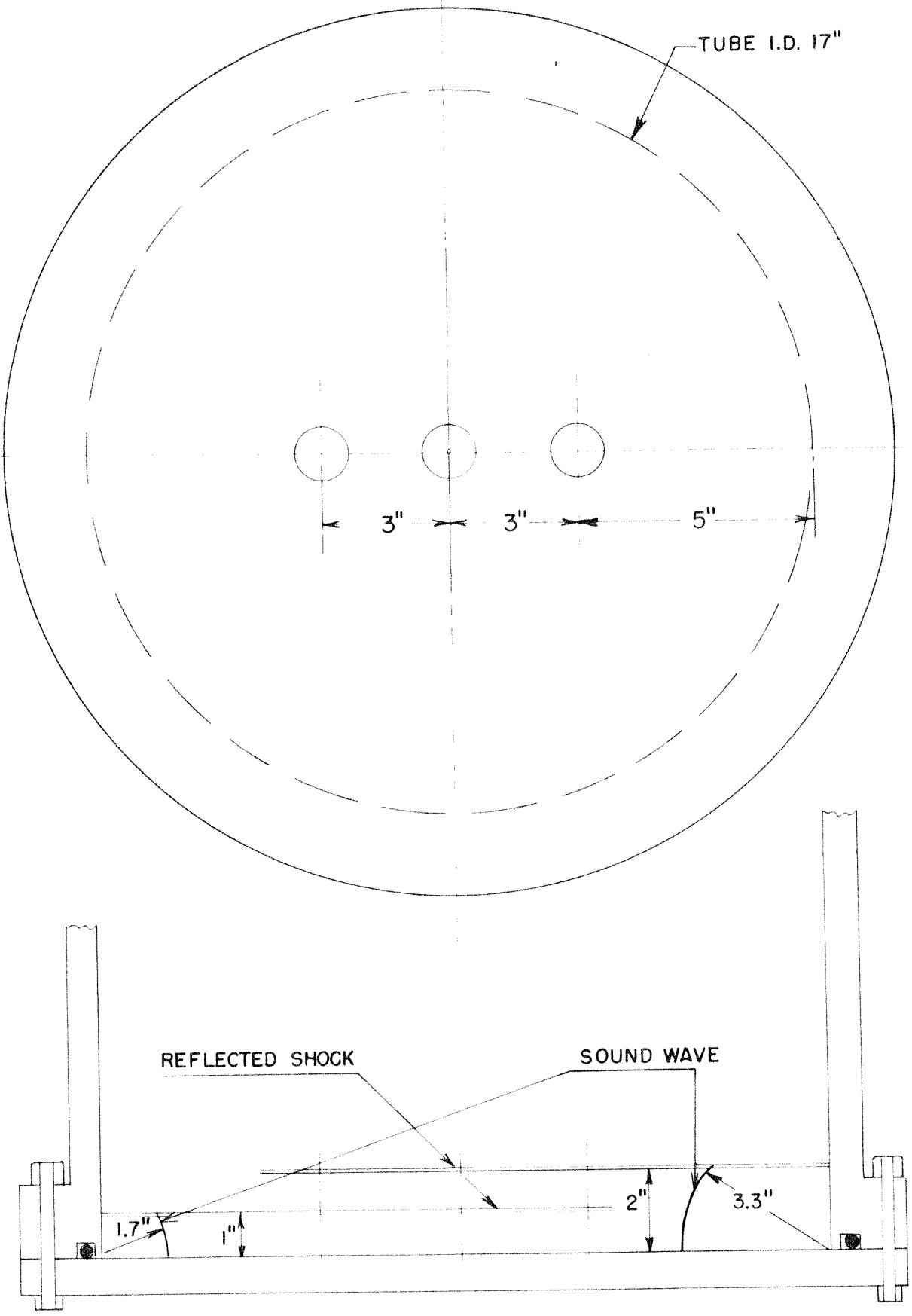

Fig. 4. Probe Location and Test Region.

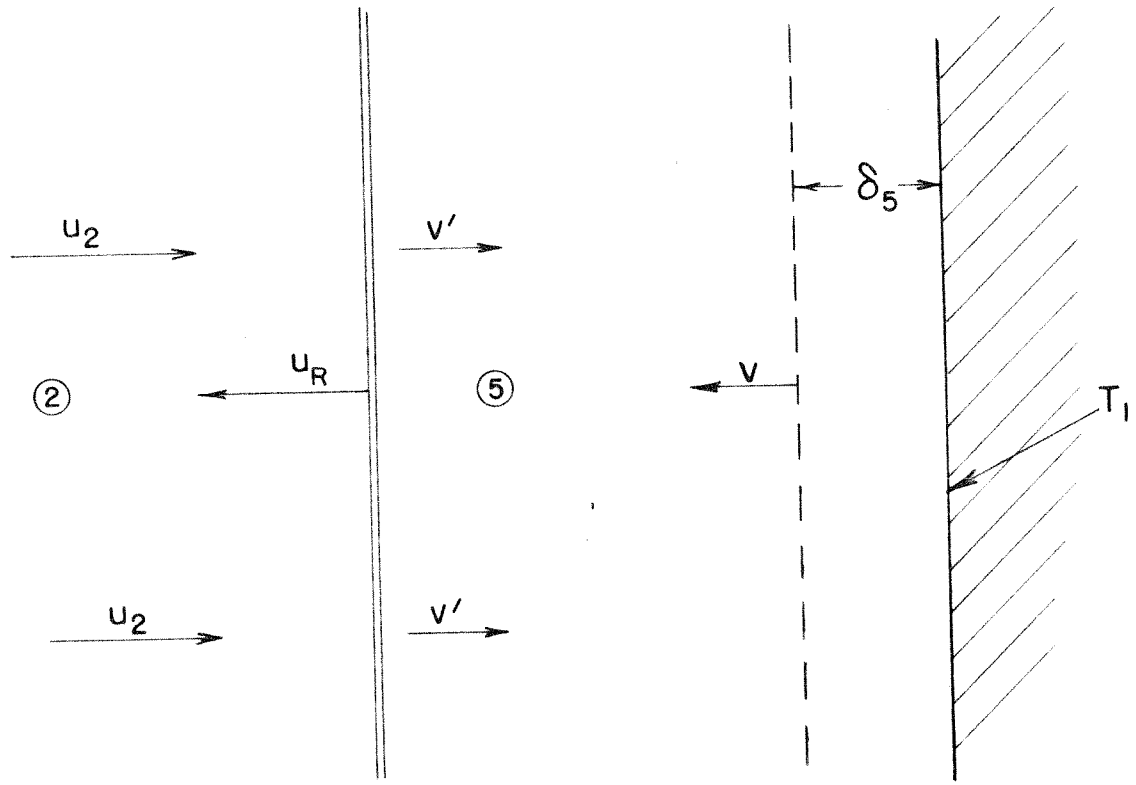

Fig. 5. Schematic Model of Reflecting Shock.

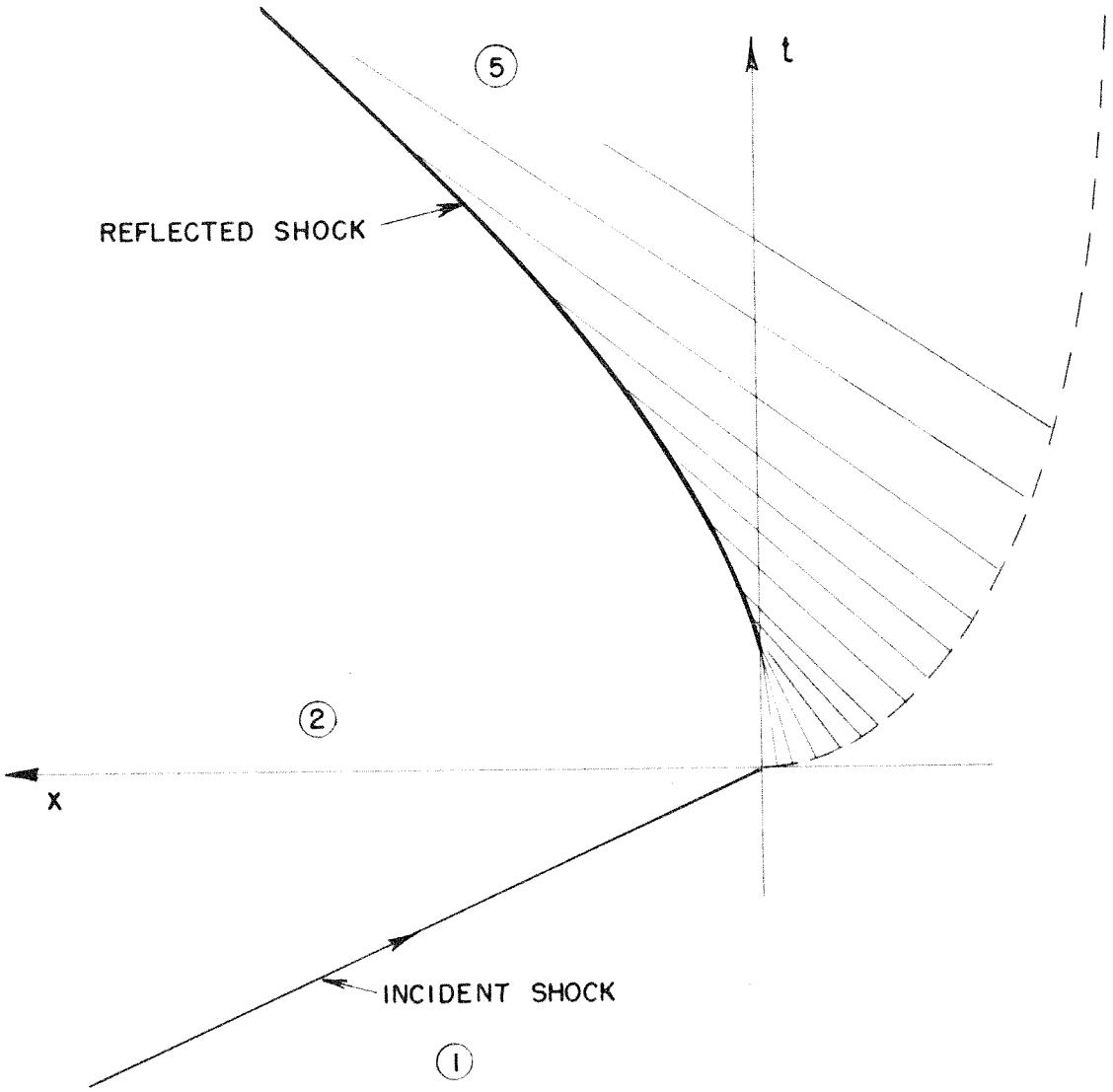

Fig. 6. x, t Diagram of Reflecting Shock.

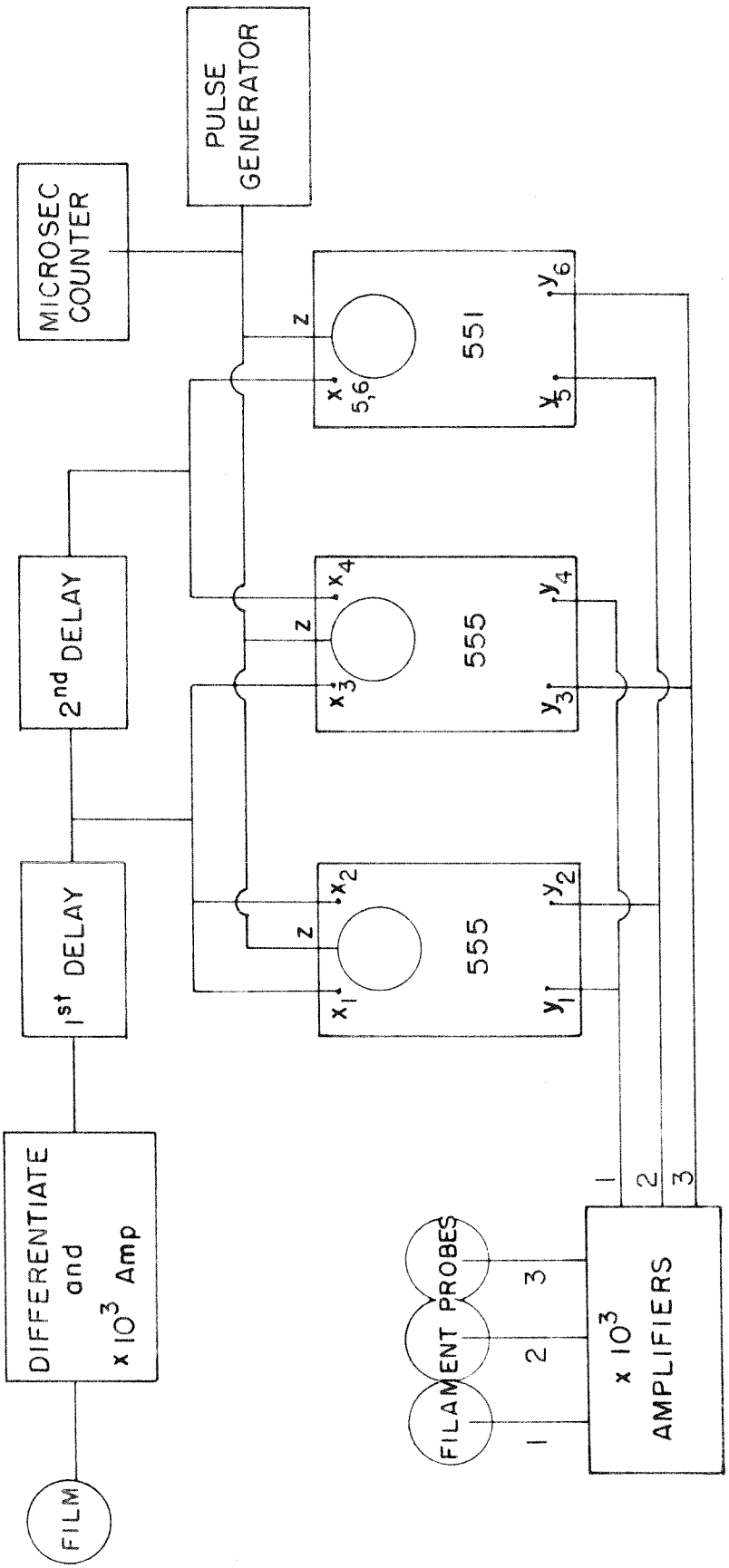

Fig. 7. Block Diagram of Instrumentation.

Beam	Probe
1	1
2	2
3	3
4	1
5	2
6	3

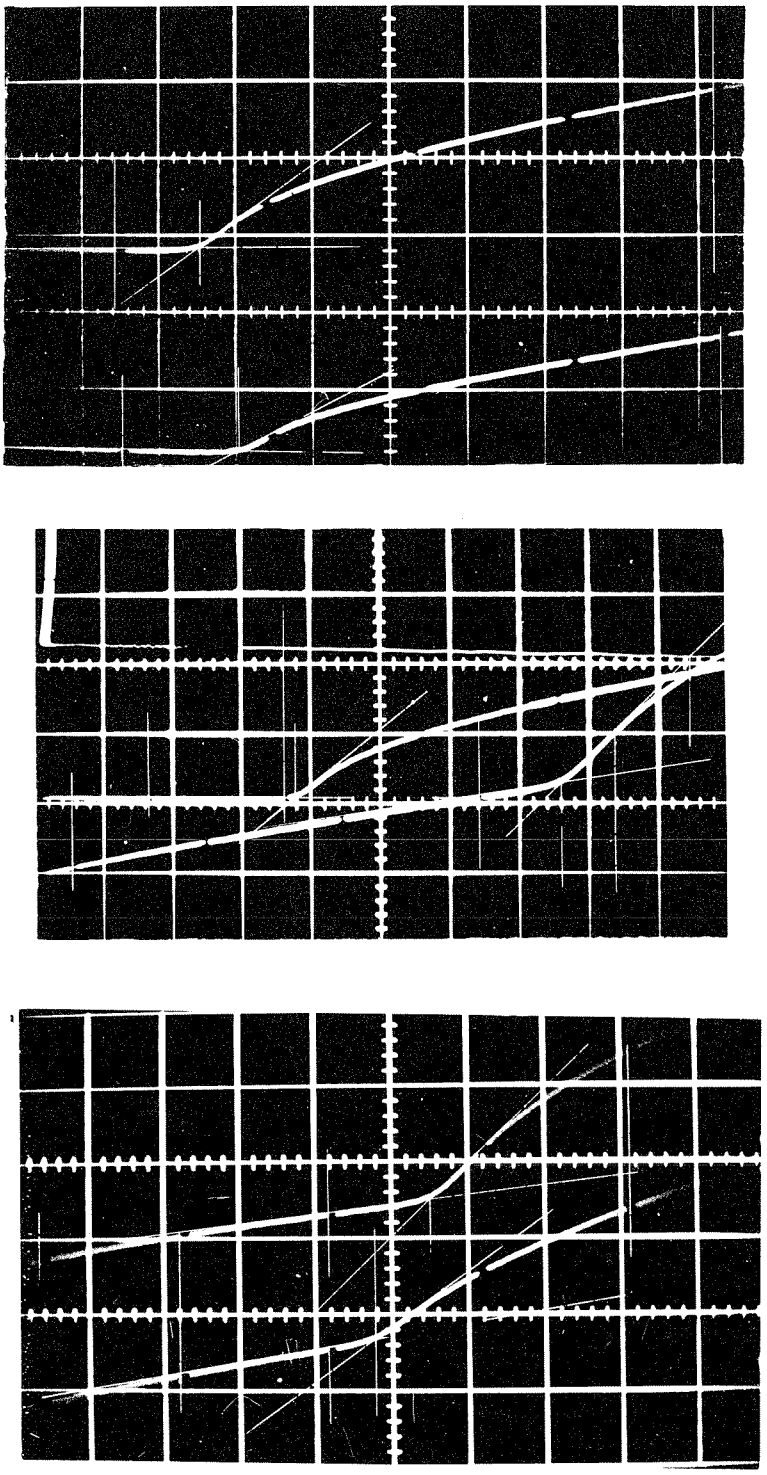

Fig. 8a. Typical Traces for Reflected Shock Measurements $p_1 = 50$ μHg, $M_s = 4.12$. Sweep speed 5 μsec/cm, vertical deflection 2 mv/cm.

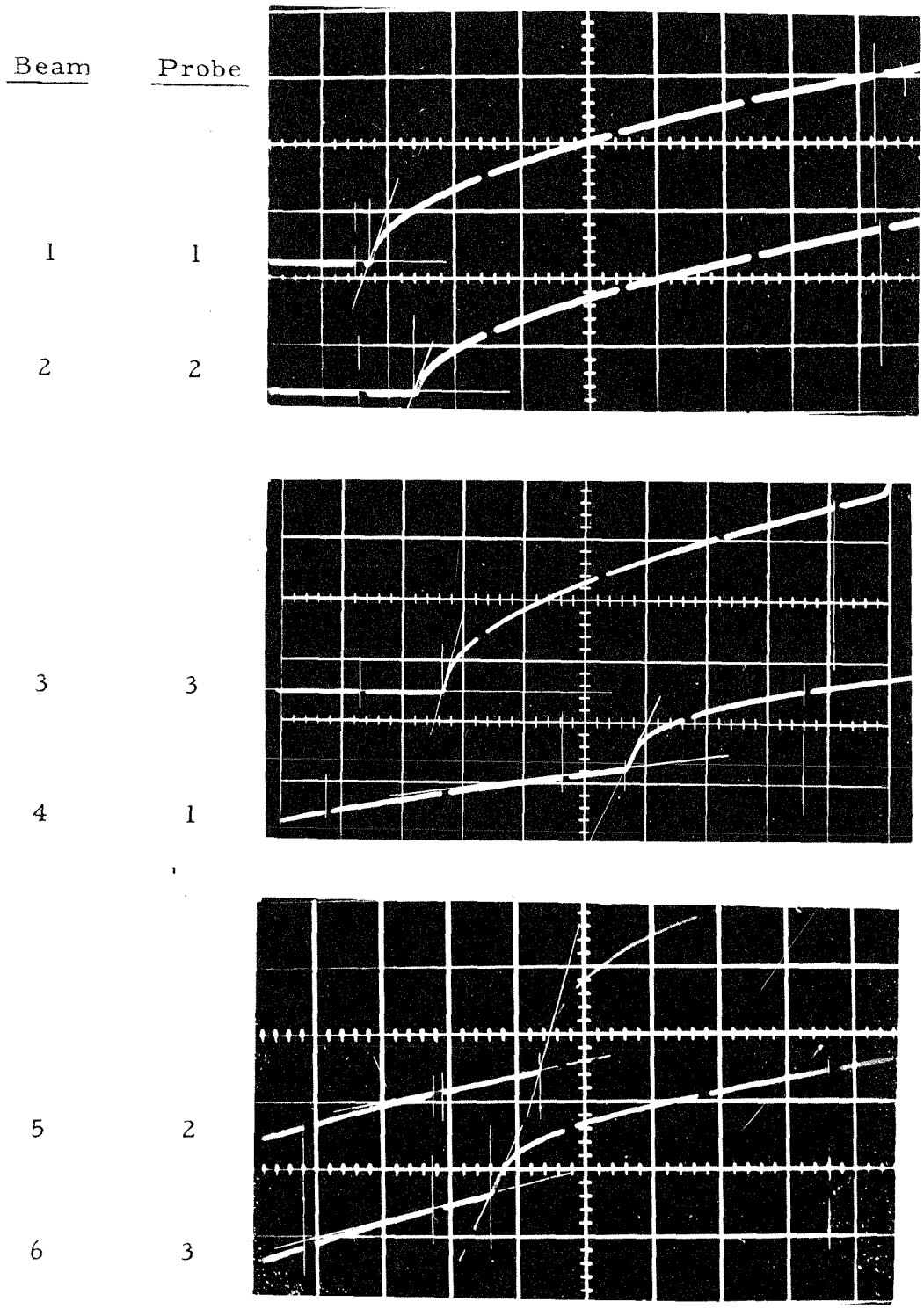

Fig. 8b. Typical Set of Traces for Reflected Shock Measurements p_1 = 500 μHg, M_s = 4.05. Sweep speed 5 μsec/cm, vertical deflection 20 mv/cm.

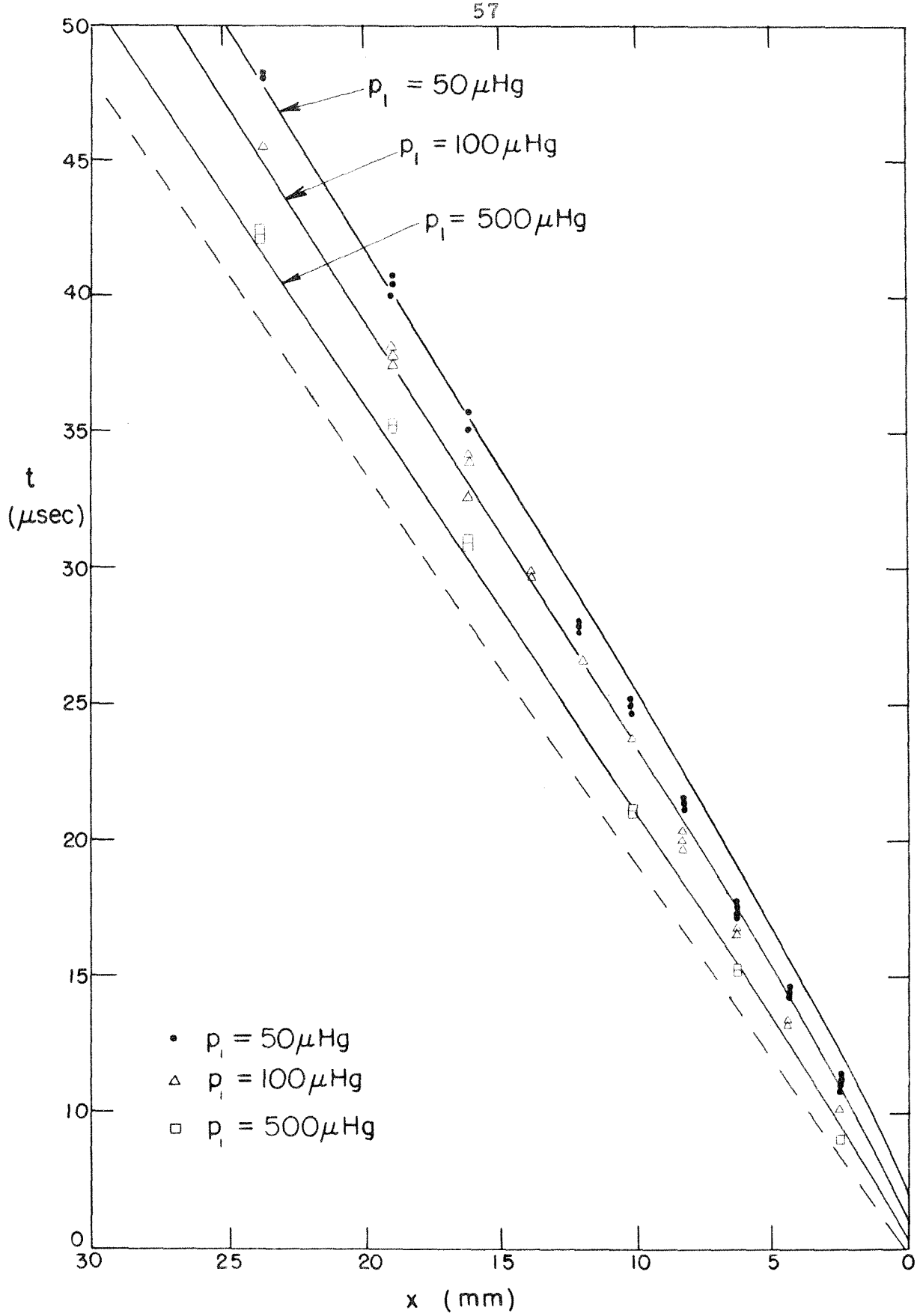

Fig. 9. Dimensional Presentation of Results.

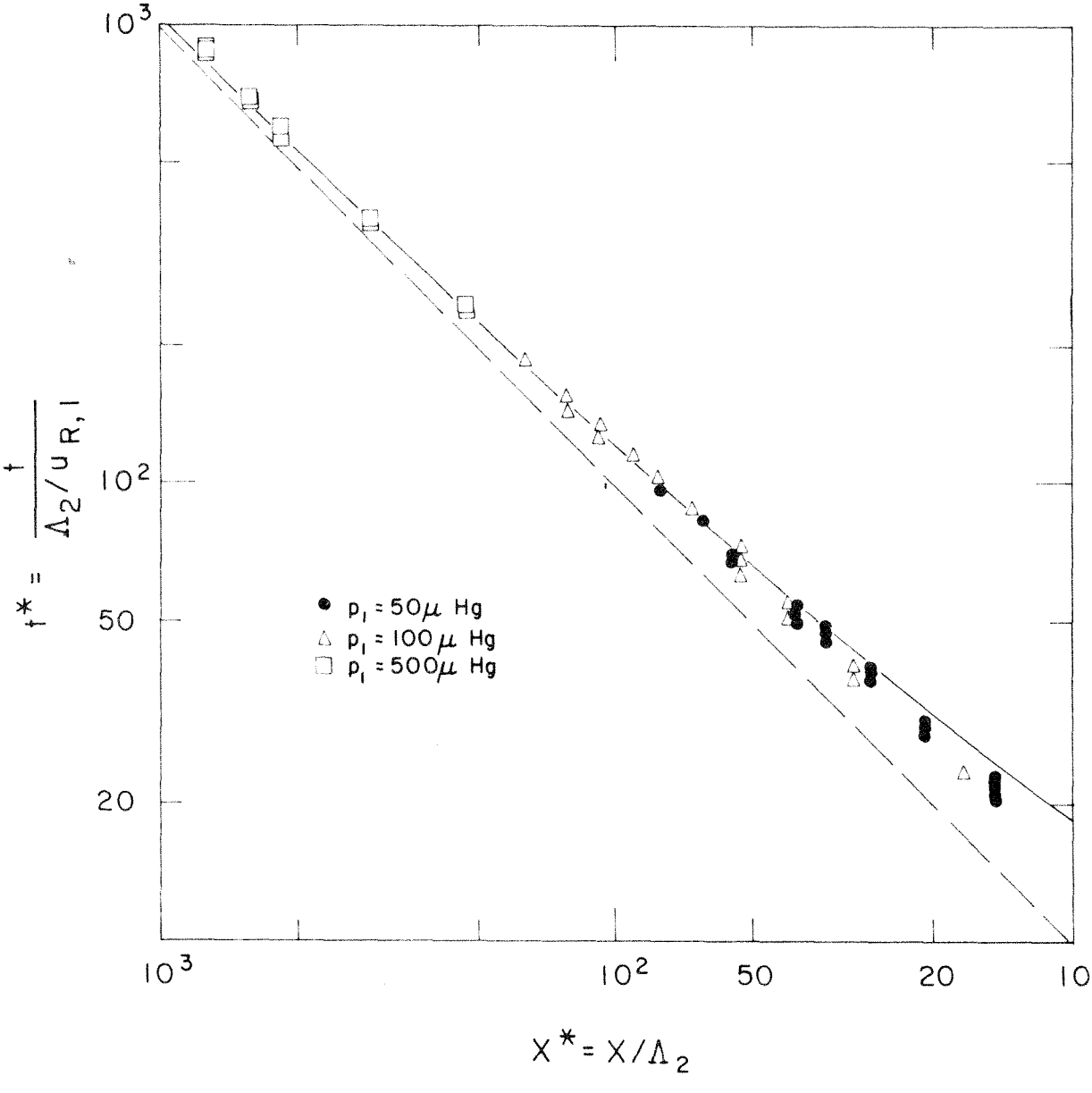

Fig. 10. Non-Dimensional Presentation of Results.

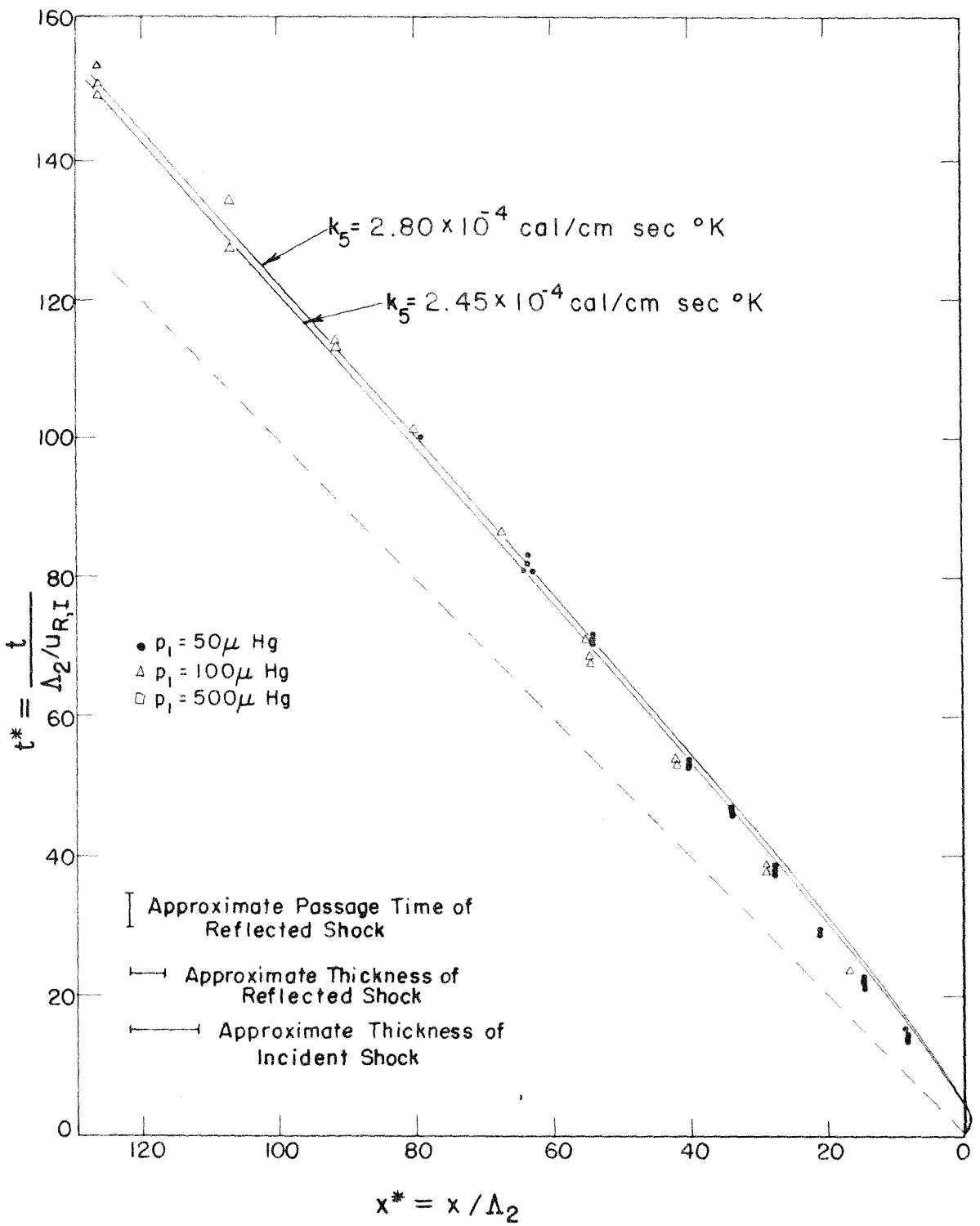

Fig. 11. Reflected Shock History Close to End Wall.